Organic Dipole Layers for Ultralow Work Function Electrodes

William E. Ford, Deqing Gao, Nikolaus Knorr, Rene Wirtz, Frank Scholz, Zoi Karipidou, Kodo Ogasawara, Silvia Rosselli, Vadim Rodin, Gabriele Nelles, and Florian von Wrochem*

Materials Science Laboratory, Sony Deutschland GmbH, Hedelfinger Strasse 61, 70327 Stuttgart, Germany

ABSTRACT The alignment of the electrode Fermi level with the valence or conduction bands of organic semiconductors is a key parameter controlling the efficiency of organic light-emitting diodes, solar cells, and printed circuits. Here, we introduce a class of organic molecules that form highly robust dipole layers, capable of shifting the work function of noble metals (Au and Ag) down to 3.1 eV, that is, ~1 eV lower than previously reported self-assembled monolayers. The physics behind the considerable interface dipole is elucidated by means of photoemission spectroscopy and density functional theory calculations, and a polymer diode exclusively based on the surface modification of a single electrode in a symmetric, two-terminal Au/poly(3-hexylthiophene)/Au junction is presented. The diode exhibits the remarkable rectification ratio of $\sim 2 \cdot 10^3$, showing high reproducibility, durability (>3 years), and excellent electrical stability. With this evidence, noble metal electrodes with work function values comparable to that of standard cathode materials used in optoelectronic applications are demonstrated.

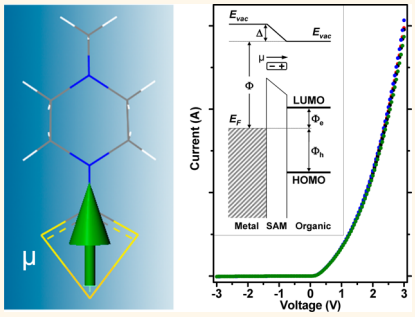

KEYWORDS: molecular dipole · self-assembled monolayer · injection barrier · organic electronics · work function · interface dipole

A significant research effort has been directed toward the control of the interface between metals and organic semiconductors,[1,2,3] in particular after the development of organic light emitting diodes (OLEDs),[4,5] organic solar cells,[6] and organic field effect transistors (OFETs).[7] The energy levels/bands of the organic semiconductor represent the channels for charge transport, and lowering the injection barrier between these transport levels and the Fermi energy of the contacts is crucial for device performance.[8] Even though device efficiency experienced a significant improvement over the past decades, the energy level alignment at electrode/semiconductor interfaces is often limited by the small number of electrode materials (having discrete Fermi energies) that are brought into contact with a wide spectrum of commercially available organic semiconductors. This particularly holds for polymer-based devices (*e.g.*, printed organic circuits and OFETs), where molecular doping and the fabrication of multilayer structures for tuning the injection barrier at the interface are not feasible.

The relative vacuum levels of metals and semiconductors have been adjusted in different ways, for example, by the deposition of a thin film of a high/low work function material on common metal electrodes.[9,10] Alternatively, the surface potential has been tuned by the physisorption of organic adsorbates forming an interface dipole at the metal surface,[1,8,11] in some cases allowing a reduction in the work function due to electron transfer from the adsorbate to the metal.[12,13] Injection barrier tuning has also been attempted using self-assembled monolayers (SAMs)[14] of molecules covalently linked to the substrate and that exhibit a permanent dipole moment. The first studies from Ferraris *et al.*[15] demonstrated that dipolar organic monolayers on metal surfaces induce a change in the work function (Φ) due to a shift Δ of the relative vacuum levels (VL) inside and outside the metal boundaries.[16,17] Since then, a growing interest in modifying the work function of electrodes using SAMs,[15,18,19] in particular for solar cells,[21] OLEDs,[22] and OTFTs,[23,24] evolved. However, a significant reduction of the metal work function using SAMs could not be achieved so far, being limited to the range from 4.0 to 5.7 eV (*e.g.*, by thiolate modification).[15,18] Recently, physisorbed polyamine modifiers have been employed by Zhou *et al.* for work function lowering.[25] Even though this approach is attractive due to its applicability to a wide range of metals, the amorphous character of the polymer and its

* Address correspondence to Florian.vonWrochem@eu.sony.com.

Received for review May 22, 2014 and accepted August 5, 2014.

Published online August 05, 2014
10.1021/nn502794z

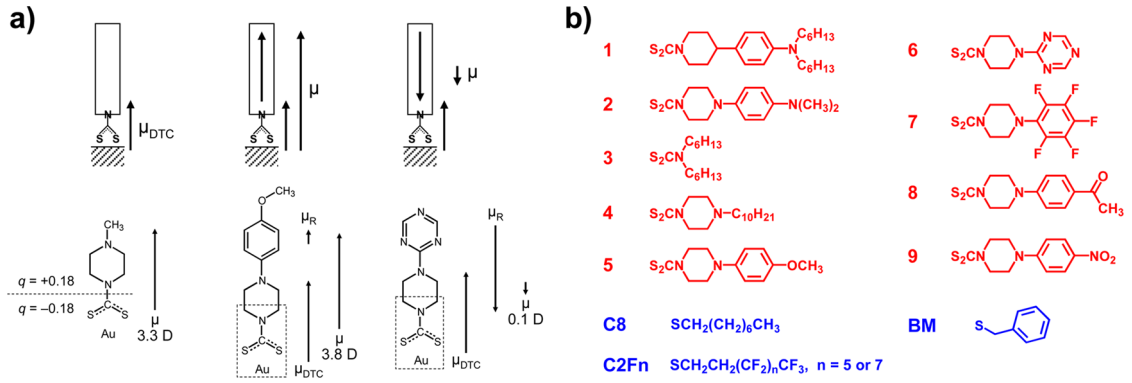

Figure 1. (a) The two main components of the molecular dipole, μ_{DTC} and μ_R, result in the total dipole moment μ of the molecular rod. The high intrinsic dipole moment μ_{DTC} stems from the shift of electronic charge from the amine group to the CS_2 moiety, expressed in a partial charge of $q = -0.18$ *e* on the CS_2Au moiety (see also Figure S2). (b) Molecular structures of the investigated DTC (red) and thiolate (blue) derivatives.

physisorption to the substrate limits the structural order and/or the stability at the interface; moreover, the work function is fixed to a particular value by the chemical nature of the polymer. In these regards, ultrathin ordered and densely packed SAMs are excellent candidates to form robust and electrically stable interfaces, besides being able to stabilize some electrode materials (*e.g.*, Ag) that are susceptible to atmospheric oxidation or corrosion.[9,26] By molecular design, SAMs can be tailored such to (i) shift the work function to specific values of Φ for the alignment of the metal Fermi level with the transport levels of a given semiconductor, and (ii) maximize the adhesion of the deposited organic semiconductor by using appropriate chemical substituents.

Here, we present a class of highly dipolar monolayers capable of reducing the work function of noble metals (Au and Ag) to values as low as 3.1 eV, thus reaching a regime known from standard cathode materials used in optoelectronic applications. The layers open a new route toward the optimization of metal–organic interfaces in organic light emitting diodes,[27] solar cells,[28] thin film transistors,[7] or printed organic circuits.[29] Notably, the monolayers are linked to noble metal substrates by a bidentate, covalent bond, allowing robust and highly reproducible contacts. Furthermore, interface dipoles as well as surface energies (adhesion) are tunable by synthesis, allowing work function control over a range of 1.6 eV and the deposition of either hydrophobic or hydrophilic organic materials. As a proof of concept, a polymer diode based on the surface modification of a single electrode in a symmetric, two-terminal Au/poly(3-hexylthiophene)/Au junction is presented. The diode reaches an unrivalled rectification ratio of $2 \cdot 10^3$, also featuring an excellent reproducibility, electrical stability, and durability (>3 years).

RESULTS AND DISCUSSION

To combine a high molecular dipole moment with a possibly dense molecular packing within the monolayer, we designed rod-shaped molecular structures having a DTC-piperazine-R or DTC-piperidine-R motif, where DTC represents a dithiocarbamate (DTC) moiety and R is an aryl or alkyl substituent. As shown in Figure 1a, the dipole moment μ of such a molecular rod can be divided in two components, μ_{DTC} and μ_R. The intrinsic dipole moment μ_{DTC} results from the strong electronegativity difference between the CS_2 moiety and the secondary amino group and amounts to ~3.3 D (see partial charges in Supporting Information, Figure S3). A second, tunable component of the dipole moment μ_R consists of the aromatic backbone substituted by a number of acceptor/donor groups that cause a redistribution of the electronic charge and a modulation of the total dipole moment. The bridge between DTC group and aromatic backbone is given by the piperidine/piperazine ring that (i) ensures the rod-like symmetry of the molecular backbone favoring a perpendicular orientation of the molecular axis on the substrate and (ii) facilitates the self-assembly process by its conformational flexibility. By molecular design, a smooth variation of μ in the range from −4.8 to 5.5 D is achieved, as verified by density functional theory (DFT) calculations for the compounds DTC **1**–**9** (Table 1 and Supporting Information, Figure S5).

Monolayers of DTC **1**–**9** (Figure 1b) are formed by the immersion of Au electrodes into ethanolic solutions containing 1 mM of the respective material.[31] Details on synthesis and preparation are provided in the Supporting Information and in the Methods section. Alkanethiol monolayers are prepared as previously reported.[30] Elemental composition, core level shifts, and molecular densities of the SAMs are obtained from X-ray photoemission spectroscopy (XPS, Figure S1) and show evidence for compact monolayers having molecular densities comparable to those of alkanethiols on Au (Table 1). The negative partial charge on the sulfur atoms, essentially contributing to the high intrinsic dipole moment of the DTC moiety, emerges from DFT calculations (Figure 1a and Supporting Information, Figure S3)

and is reflected in a shift of the XPS sulfur 2p signal to lower binding energies (Figure S1a).[31] Importantly, the tilt angle of the molecular axis relative to the surface normal must be well-known to allow conclusions on the electrostatic potential drop at the interface. Thus, the molecular density of the SAM is obtained from XPS data (Table 1) and then given as an input to DFT calculations, allowing an estimation of the molecular tilt angle within the monolayer. From the computational model, a nearly perpendicular orientation of the molecular backbone toward the surface plane is deduced for most DTC monolayers (see Figure S4), such that a linear dependence of the interface dipole Δ on μ_z is expected (based on the Helmholtz equation $\Delta = \mu_z \cos\alpha/\varepsilon_0 A$, where μ_z is the dipole moment along the molecular axis, ε_0 is the vacuum permittivity, A is the molecular area, and α is the tilt angle of the molecular axis toward the surface normal).

TABLE 1. Core Level Binding Energy, Molecular Density, Dipole Moment, and Work Function for DTC and *n*-Alkanethiol Compounds Deposited on Au Substrates (in the Order of Dipole Moment Magnitude). The Values Are Derived from XPS/UPS Data and from DFT Calculations

compound	S 2p[a] (eV)	C 1s[a] (eV)	density[b]	μ_z[c] (Debye)	μ[c] (Debye)	Φ[d] (eV)
1	161.98	285.05 (286.0)	0.77	5.54	5.88	3.22
2	161.82	284.79 (285.9)	1.18	4.76	4.98	3.23
3	161.89	284.61 (285.6)	0.47	3.85	3.89	3.58
4	161.81	285.56	0.892	3.67	3.72	3.44
5	162.00	285.25 (286.2)	1.06	3.52	3.78	3.52
6	161.92	285.99 (287.3)	1.015	−0.06	0.11	4.43
7	161.87	286.07 (286.9)	1.095	−0.21	0.48	4.33
8	161.77	284.63 (285.8)	0.907	−1.48	2.61	4.51
9	161.85	284.94 (286.0)	0.76	−4.76	5.19	4.75
n-octanethiol	162.08	284.9	0.93	0.82	1.76	4.12

[a] Binding energy for S 2p and C 1s core level signals in units of eV gained from XPS. In parentheses, the second component of the C 1s signal is given. [b] Molecular density derived from S 2p/Au 4f and N 1s/Au 4f ratios, representing an average from several measurements with different samples. These values are referred to the respective ratio from densely packed dodecanethiol monolayers (0.045), which is defined here as a standard due to its well-known molecular density.[32] [c] Molecular dipole moment (in Debye) computed from gas-phase DFT calculations of single molecules (coordinated to a single Au atom) at the BLYP level. The component of the dipole moment along the molecular axis, μ_z, and the absolute dipole moment, μ, are listed. [d] Work function of an atomically flat TSG surface modified with a dense SAM of the respective compound. The values are obtained from the low kinetic energy photoemission threshold (secondary photoemission cutoff) in the UP spectra (Figure 2a) and are referenced to a freshly sputtered Au surface (Φ_{Au} = 5.12 eV).

The work function Φ of the modified Au/Ag surfaces is obtained by ultraviolet photoemission (UP) spectroscopy, which provides the valence band structure both of the solid and of the interface. From $h\upsilon = W + \Phi$, where υ is the frequency of the source and W is the difference between the Fermi energy and low kinetic energy photoemission cutoff, Φ is obtained.[16] The cutoff region for DTC-**1**, *n*-octanethiol (C8), and sputtered Au (Φ_{Au} = 5.12 eV) is shown in Figure 2a. The values of Φ obtained upon Au-modification with nine DTC compounds (Table 1) are correlated in Figure 2b with molecular dipole moments from DFT calculations. A nearly linear dependence of Φ on μ_z is observed, where Φ extends over a range of ~1.6 eV and reaches down to Φ = 3.2 eV. As a reference, the dependence of Φ on μ_z for known fluorinated and nonfluorinated thiolate derivatives is presented in Figure 2b (inset). Deviations from linearity are interpreted in terms of small variations in surface density, molecular conformation, or orientation within each monolayer. Also, depolarization effects from intermolecular electrostatic interactions are expected to affect the interface dipole in densely packed monolayers,[33] which might in part explain the smaller Φ/μ_z slope that we observe for aromatic DTCs (−0.20 eV/Debye) compared to aliphatic thiolates (−0.35 eV/Debye).[34] Notably, DTC monolayers on Ag substrates present a similar Φ/μ_z correlation (Figure 3), however showing slightly lower work function values compared to Au substrates

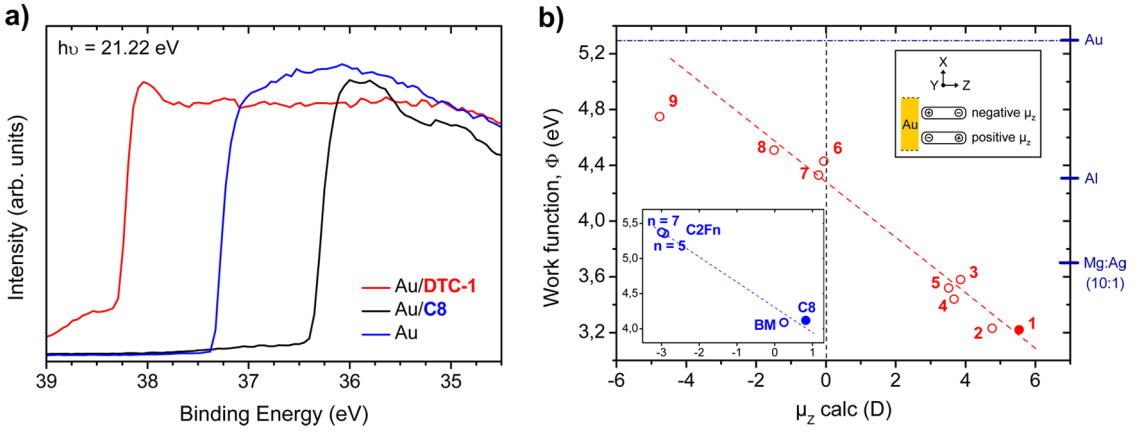

Figure 2. (a) Secondary photoemission cutoff as acquired by UPS (He I, 21.22 eV), yielding the work function of the modified Au surface. Monolayers of DTC-1 (red) and *n*-octanethiol (C8, blue) are compared with the spectrum of a clean, sputtered Au surface (black) with Φ_{Au} = 5.12 eV. (b) Dependence of the work function Φ (from UPS) on the dipole moment μ_z (from DFT calculations) for nine DTC derivatives investigated in this study. An analogue graph for thiolate monolayers (blue structures in Figure 1b) is shown as an inset. As a reference, relevant values of Φ for commonly used metals and alloys are shown on the right ordinate.

(*e.g.*, 3.1 eV for DTC-**2**). This finding is relevant in view of the common use of Mg:Ag alloys ($\Phi \sim 3.7$ eV) and of Ca/Ag and Mg/Ag double layers as cathode materials in optoelectronic applications (*e.g.*, OLEDs),[4,9] where DTC dipole layers might become a valid alternative to alkaline earth metal coatings in future applications.

As a proof of concept, we verified the impact of DTC-based interface dipoles on device performance by electrical measurements of poly(3-hexylthiophene) (P3HT) diodes having the structure Au/monolayer/P3HT/Au (Figure 4a). The devices are prepared by the evaporation of bottom electrodes on Si/SiO_2 wafers and, after SAM modification, by P3HT spin-coating from a trichlorobenzene solution to form 100 nm thick, continuous polymer films. Top electrodes are subsequently deposited on the P3HT layer, resulting in cross-point junctions having dimensions of 100 μm $\times$ 100 μm (Figure 4a, inset). The P3HT junctions are either stored under high-vacuum (HV) conditions for a few days or thermally annealed before being bonded and transferred to the cryostat (pressure: 10^{-6} mbar), where they are measured at room temperature following a storage time of about 1 week. In Figure 4b, the current density−voltage ($J-V$) characteristics of P3HT junctions realized with DTC-**1** and C8 monolayers are shown (Φ = 3.2 and 4.1 eV, respectively). As a reference, junctions with two unmodified Au electrodes as well as Al/P3HT/Au junctions having one aluminum contact were prepared. Note that the additional native AlO_x layer on the aluminum surface acts as a tunneling barrier, leading to drastically reduced current densities (*vide infra*).

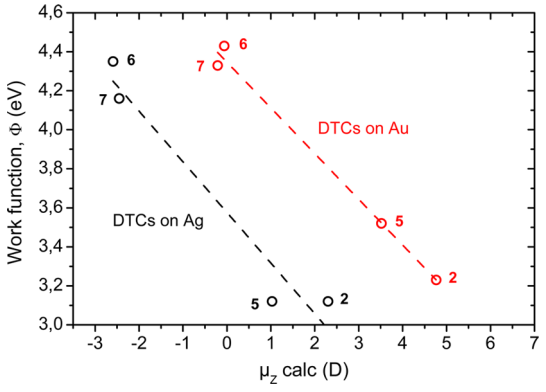

Figure 3. Correlation of work function Φ (from UPS) and dipole moment μ_z (from DFT calculations) for five DTC derivatives on Ag and Au substrates. The work function difference for Au and Ag substrates, modified with equal DTCs, is lower than expected based on the nominal work function difference of the two metals (Φ_{Au} = 5.3 eV, Φ_{Ag} = 4.5 eV). This effect has been observed experimentally for alkanethiols on Au and Ag by de Boer *et al.*[19] and was explained theoretically by Heimel *et al.*[20]

As shown in Figure 4b, the rectification ratio (RR) of the diode (at $\pm$3 V) increases from RR $\approx$ 1 for symmetric contacts in Au/P3HT/Au junctions, to a value of 2×10^3 for Au/DTC-**1**/P3HT/Au junctions. In the latter case, an ideal diode behavior is observed, with a negligible scattering of current densities among multiple junctions (Figure 4a, main graph). For Au/C8/P3HT/Au junctions, no asymmetry in the $J-V$ curves is found, but J is lower by 1 order of magnitude compared to Au/P3HT/Au reference junctions. Diodes with the structure Al/P3HT/Au, having asymmetric contacts, show a RR of $\sim 2 \times 10^4$ with the same polarity as in case of Au/DTC-**1**/P3HT/Au junctions, but with J attenuated by a factor of $\sim 10^3$ (relative to Au/P3HT/Au).

These results can be rationalized in terms of two contributions: (1) the effect of tunnelling barriers on the magnitude of J and (2) the rectification arising from the energy level alignment/misalignment at the two contacts. First, the attenuation of J depends on the thickness of the molecular/oxide layer at the

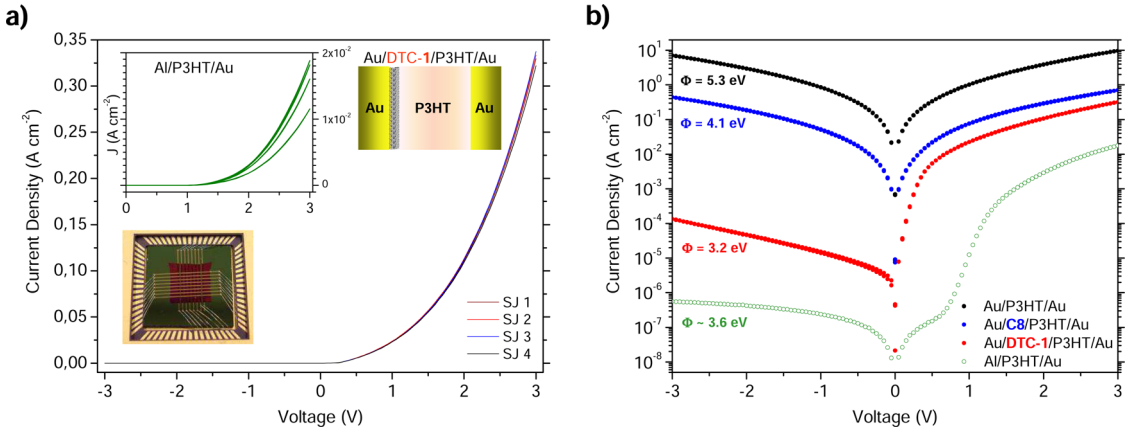

Figure 4. (a) Diode characteristics from junctions with the structure Au/DTC-1/P3HT/Au (the layer structure is shown in the upper right inset). In the left inset, $J-V$ characteristics from the structure Al/P3HT/Au are presented for comparison. The standard deviation of J (at +3 V) from the mean is 2% for Au/DTC-1/P3HT/Au junctions and 20% for Al/P3HT/Au junctions. The lower inset shows the crossbar structure mounted on a chip carrier. (b) Semilog plot showing the averaged $J-V$ curves for Au/SAM/P3HT/Au and Al/P3HT/Au junctions, as well as for Au/P3HT/Au reference junctions (black data points). At positive bias, the black, blue, and red curves obey the trap-free space charge limited current (SCLC) injection behavior. The Al/P3HT/Au junction (green data points) obeys Ohm's law below 0.8 V, whereas it shows a steep increase at V_{TFL} = 0.8 V. The transition marks the trapped filled limit[44] related to the presence of traps in the oxide layer (Supporting Information, Figure S5).

metal/P3HT interface. P3HT is known to forms crystals having both the polymer chain axis and the π-stacking direction of the polymer in the plane of the film, at least if the regioregularity of P3HT is >91%.[35] This holds even more if P3HT has been spin-coated on alkylated surfaces,[36] as they preferentially interact with the hexyl chains of the P3HT backbone. The presence of alkyl chains in C8 and DTC-**1** monolayers supports this interaction, but also increases the tunneling distance between the P3HT crystals and the Au surface, causing a reduction of J (compared to Au/P3HT/Au junctions) as observed in Figure 4b. For junctions with one aluminum contact (Al/P3HT/Au), J dramatically drops by a factor of 10^3, in quite good agreement with the known dependence of the electrical resistance on the oxide thickness of aluminum (~1 decade/nm),[37] because AlO_x is known to be ~3 nm thick. Note that whereas most metals are subject to oxidation, severely limiting current injection, DTC monolayers can be made as thin as 6 Å (see Figure S3), which minimizes the impact of tunnelling barriers on device performance.

In the following, we will consider in detail the effects arising from energy level alignment/misalignment at the contacts. Figure 5 shows the relevant energy level diagrams based on our spectroscopic data for Au/C8 and Au/DTC-**1** interfaces, and based on literature for the P3HT/Au interface. The work function of crystalline Au is 5.3 eV,[38] whereas for Al with a native oxide layer it is reported to range from 3.2 eV[39] to 3.9 eV.[2] Upon P3HT spin-coating, the work function of Au is known to be reduced to ~4.0 eV.[40] This work function reduction is mainly related to the push-back effect,[1] that is, to the suppression of the electron density tail at the metal surface, although an additional interface dipole arising from charge transfer at the P3HT/Au interfaces was reported.[40] For Au substrates coated with C8 and DTC-**1** SAMs, the work functions are reduced to 4.1 and 3.2 eV, respectively (Figure 2b and Table 1). These shifts result from a combination of the push-back effect and the interface dipole created by the chemisorbed monolayer. With an ionization potential (IP) of 4.6 eV for P3HT films, that we determined by adding the work function of the Au/C8/P3HT substrate (Φ = 4.0 eV) to the highest occupied molecular orbital (HOMO) threshold of P3HT (ϕ_b = 0.58 eV, see Figure S2) and that is found to be in line with recently reported values for P3HT films measured on flat substrates (IP = 4.7 eV),[41] an energy diagram as shown in Figure 5a can be drawn. Here, we have assumed for P3HT a band gap of 2.2 eV[42] (from electrochemical measurements) and a hole injection barrier of ~0.58 eV (as obtained from UPS data, see Figure S2a). Having these figures in mind, P3HT is regarded as a hole conductor both in Au/P3HT/Au and in Au/C8/P3HT/Au junctions, in particular as the hole injection barrier obtained for the Au/C8/P3HT interface is almost identical to the value reported for the Au/P3HT contact (ϕ_b = 0.6 eV).[38,43]

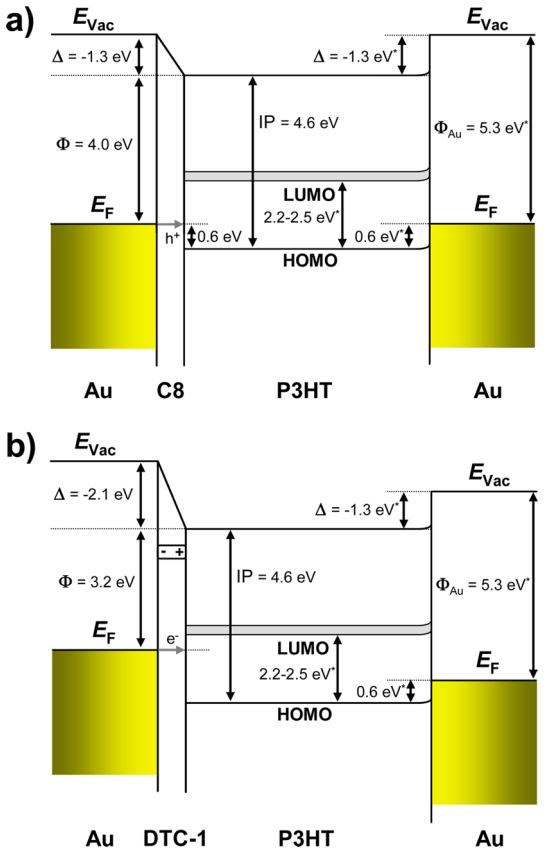

Figure 5. (a) Energy level diagram illustrating the band alignment in Au/C8/P3HT/Au and (b) Au/DTC-1/P3HT/Au junctions as obtained from UP measurements. The band structure at the P3HT/Au interface (right side), *i.e.*, the values denoted by an asterisk, are taken from literature (see text). Ohmic injection into the HOMO (LUMO) levels of the organic semiconductor occurs if the Fermi level E_F is nearly aligned with the semiconductor hole (electron) transport levels.[2] The alignment at the left electrode is controlled by the interface dipole Δ arising from the molecular dipole layer.

On the basis of the above analysis and on the scheme shown in Figure 5a, no asymmetry is expected for $J-V$ curves from Au/C8/P3HT/Au devices (Figure 4b). However, the DTC-**1** monolayer induces an extraordinarily large VL shift ($\Delta = -2.1$ eV), moving the lowest unoccupied molecular orbital (LUMO) of P3HT (i.e., the electron transport level), toward the Fermi level of Au and therefore creating a Schottky barrier for hole injection from the left contact into P3HT (Figure 5b). At forward bias, the Fermi level of the right (left) electrode is lowered (raised), and holes (electrons) can be injected from the right (left) electrode. As for Au/P3HT/Au junctions, in this case space charge limited currents (SCLC) occur, expressed by the square law $J \approx \varepsilon\varepsilon_0\mu(V^2/d^3)$.[44] The SCLC regime is observed at positive bias in Figure 4b (for a detailed curve analysis see Figure S6). At reverse bias, the Fermi energy is raised (lowered) at the right (left) electrode. Thus, at both contacts Schottky barriers for electrons and holes are introduced, blocking charge injection into the semiconductor (negative bias range

in Figure 4b). Finally, for Al/P3HT contacts, an energy level diagram similar to that shown in Figure 5b (for the Au/DTC-**1** interface) applies. This means that at forward bias hole (electron) injection is possible from the right (left) contact, whereas at reverse bias both contacts are Schottky-barriers. Consistently, Al/P3HT/Au and Au/DTC-**1**/P3HT/Au junctions show a comparable asymmetry in the $J-V$ characteristics, despite the pronounced difference in absolute current magnitude due to the additional oxide layer for Al/P3HT interfaces. Note that only for Al/P3HT/Au junctions a characteristic signature for trap state filling is observed, attributed to defects at the AlO_x/P3HT interface (Figure 4b). The nearly ideal diode behavior for Au/DTC-**1**/P3HT/Au junctions, on the contrary, indicates low trap densities resulting from the highly defined/ordered metal/polymer interface. A detailed analysis of the $J-V$ characteristics is found in the Supporting Information.

A remarkable property of DTC-based polymer diodes is their significant lifetime under regular $J-V$ cycling, as well as their high stability and reproducibility over the test period in our laboratory. Monolayer-based P3HT diodes produced reliable data over more than 3 years (see Figure S7), whereas junctions with the structure Al/P3HT/Au had an average lifetime of ~3−4 weeks, before breakdown occurred due to electrical shorts. As shown in Figure 4a, a standard deviation (SD) of ~2% is determined for Au/DTC-**1**/P3HT/Au junctions, whereas Al/P3HT/Au diodes show a significantly higher SD in the range of 20%. The high SD is attributed to structural defects of the AlO_x layer, chemical reactions, and contaminants at the Al/P3HT interface. DTC based monolayer/polymer contacts offer specific structural advantages that are highly relevant in view of device performance, for example, (i) the covalent, bidentate bonding of DTCs to noble metals, offering a higher stability than other monolayers and chemisorbed polymers, (ii) the stabilizing and blocking action of dense monolayers at metal surfaces, that prevent chemical reactions,[45] the formation of gap states (traps),[46] shorts from metal filaments, and ion diffusion into the organic semiconductor, (iii) the dispersive attractive interaction among the alkyl chains of the SAM and of the polymer, that increases the adhesion and structural order at the Au/polymer interface[36] (besides enabling the facile removal of adventitious contaminants from alkyl-modified surfaces, *e.g.*, during spin-coating), (iv) the well-defined structure and molecular orientation within the SAM, resulting in a homogeneous potential profile across the interface and, as a consequence, in more reliable and reproducible electrical device characteristics, and (v) the selective deposition of dipole layers on noble metal electrodes rather than on other (undesired) device areas (*e.g.*, gate oxides in OTFTs).

CONCLUSION

We have shown that DTC dipole layers extend the work function of noble metals to very low values, enabling electron injection into the LUMO of organic semiconductors as well as the precise adjustment of the interface energetics by molecular design. The lack of oxide layers and the high degree of structural order at the metal/monolayer interface reduces both the trap density and the ohmic resistance at metal/semiconductor contacts, thus improving device performance. Even though DTCs are applicable to a smaller range of metals than polymeric surface modifiers,[25] they are structurally and chemically highly defined, which is important in view of device reproducibility (in particular as the polymers used Zhou *et al.*[25] in are known to contain water, residues from catalysts, and additives[47]).

In view of organic optoelectronic applications, DTC adlayers can be adopted in all device architectures where the interface energetics needs to be adjusted in between the bottom contact and the semiconductor, for example, in top emitting OLEDs (especially inverted top emitting OLEDs, where the bottom contact is the cathode),[27,48] in n-type OFETs (bottom source and drain contacts),[7,49] in organic solar cells[28] (for maximizing V_{oc}), or in printed organic circuits. In the latter case, metal oxidation and/or contamination during the printing process (often carried out under ambient conditions) can be prevented. As the electrode modification using SAMs involves a simple solution-phase deposition process, the method is in line with the requirements from industry for the manufacturing of low cost, organic printed electronic devices.

METHODS

Device Preparation. Template stripped gold (TSG) surfaces for spectroscopic investigations are prepared using known procedures (Supporting Information). For electrical measurements, 100 μm wide bottom electrodes are realized by the vacuum evaporation of 5 nm Cr and 50 nm Au on a Si wafer. Dithiocarbamates are either isolated as salts and self-assembled from solution or grown by immersing metal substrates into solutions of carbon disulfide and the organic amine. The dithiocarbamate monolayers **1**−**9** are formed under inert conditions immersing the substrates into a 1 mM ethanolic solution (argon saturated) of the respective compound for ~24 h.[31,50,51,52] Subsequently, P3HT is spin-coated from a trichlorobenzene solution to form a 100 nm thick film with a root-mean-square roughness of ~20 nm. Top electrodes are deposited by the evaporation of 55 nm of Au with the shadow mask rotated by 90°. The chips are mounted onto 10 mm × 10 mm chip carriers, and crossbar electrodes are bonded with Al-wires with a diameter of 25 μm.

UP Spectroscopy. UP spectra are obtained using a He I light source ($h\upsilon$ = 21.22 eV). The light is incident at an angle of 55° from the sample normal and the photoelectrons are collected by an energy dispersive hemispherical analyzer at a takeoff angle of 90°. The analyzer is set to a pass energy of 5 eV, providing an instrumental resolution of about 0.14 eV. Binding

energies are referenced to the Fermi level of a clean, argon ion-etched Au surface and defined as positive for occupied states below the Fermi level.

XP Spectroscopy. XP spectra are recorded with a Kratos Axis Ultra instrument using an Al Kα (1486.6 eV) line as a source. With an X-ray monochromator and a pass energy of 40 eV for the analyzer an instrumental resolution of ~0.5 eV is achieved.

DFT Calculations. Single molecule calculations are done at the BLYP theory level employing a double numerical basis set with polarization functions (DNP). For core electrons, density functional semicore pseudopotentials (DSPP) are employed. DFT calculations with periodic slab models are done using the PBE functional. To include dispersion forces, a hybrid semiempirical solution following a scheme from Tkatchenko and Scheffler is used (see Supporting Information). All calculations are done with the program Dmol[4] (Accelrys) using a convergence tolerance of 10^{-5} Hartree.

Electrical Characterization. Electrical data are acquired under high vacuum (HV) conditions (base pressure, 10^{-6} mbar) and at room temperature using a modified optical cryostat (Oxford Optistat CF-V) and a custom built, automated data acquisition system driven by a Hewlett-Packard/HP 4142B Modular DC Source/Monitor. The automated collection of a predefined number of traces (35 for each cross-point) over different voltage ranges (±0.5, ±1, ±2, ±3 V) for all junctions in sequence is carried out. To remove crosstalk, top electrodes are cut such that single rows can be addressed. Thus, 10 cross-points for each sample are measured resulting in 350 traces/array. Each *I*−*V* trace is acquired using a bias interval of 50 mV and an elapsed time of 120 ms for each voltage step, corresponding to a scan rate of 0.42 V/s. Averaged curves represent the mean of all single traces from multiple junctions excluding those junctions that are shorted. The samples are kept in HV for several days before characterization in order to reduce H_2O and O_2 content in the device.

Conflict of Interest: The authors declare no competing financial interest.

Supporting Information Available: Synthesis procedures, details on device preparation, XP and UP spectra, DFT calculations, and further electrical data. This material is available free of charge via the Internet at http://pubs.acs.org.

Acknowledgment. The authors gratefully acknowledge H. J. Queisser and H. Riel for helpful discussions, as well as M. Sarpasan for engineering the automated data acquisition system. Furthermore, we thank one of the referees for the constructive feedback. The paper is based in part on research supported by the FP7 project MMM@HPC EC.

REFERENCES AND NOTES

1. Ishii, H.; Sugiyama, K.; Ito, E.; Seki, K. Energy Level Alignment and Interfacial Electronic Structures at Organic/Metal and Organic/Organic Interfaces. *Adv. Mater.* **1999**, *11*, 605–625.
2. Braun, S.; Salaneck, W. R.; Fahlman, M. Energy-Level Alignment at Organic/Metal and Organic/Organic Interfaces. *Adv. Mater.* **2009**, *21*, 1450–1472.
3. Koch, N. Organic Electronic Devices and Their Functional Interfaces. *Chemphyschem,* **2007**, *8*, 1438–1455.
4. Tang, C. W.; VanSlyke, S. A. Organic Electroluminescent Diodes. *Appl. Phys. Lett.* **1987**, *51*, 913–915.
5. Burroughes, J. H.; Bradley, D. D. C.; Brown, A. R.; Marks, R. N.; Mackay, K.; Friend, R. H.; Burns, P. L.; Holmes, A. B. Light-Emitting-Diodes Based on Conjugated Polymers. *Nature* **1990**, *347*, 539–541.
6. Tang, C. W. Two-Layer Organic Photovoltaic Cell. *Appl. Phys. Lett.* **1986**, *48*, 183–185.
7. Sirringhaus, H. Device Physics of Solution-Processed Organic Field-Effect Transistors. *Adv. Mater.* **2005**, *17*, 2411–2425.
8. *Conjugated Polymer and Molecular Interfaces*; Marcel Dekker: New York, Basel, 2002.
9. Pode, R. B.; Lee, C. J.; Moon, D. G.; Han, J. I. Transparent Conducting Metal Electrode for Top Emission Organic Light-Emitting Devices: Ca−Ag Double Layer. *Appl. Phys. Lett.* **2004**, *84*, 4614–4616.
10. Baigent, D. R.; Marks, R. N.; Greenham, N. C.; Friend, R. H.; Moratti, S. C.; Holmes, A. B. Conjugated Polymer Light-Emitting-Diodes on Silicon Substrates. *Appl. Phys. Lett.* **1994**, *65*, 2636–2638.
11. Hill, I. G.; Schwartz, J.; Kahn, A. Metal-Dependent Charge Transfer and Chemical Interaction at Interfaces between 3,4,9,10-Perylenetetracarboxylic Bisimidazole and Gold, Silver and Magnesium. *Org. Electron.* **2000**, *1*, 5–13.
12. Lindell, L.; Unge, M.; Osikowicz, W.; Stafstrom, S.; Salaneck, W. R.; Crispin, X.; de Jong, M. P. Integer Charge Transfer at the Tetrakis(dimethylamino) Ethylene/Au Interface. *Appl. Phys. Lett.* **2008**, *92*, 163302.
13. Bröker, B.; Blum, R. P.; Frisch, J.; Vollmer, A.; Hofmann, O. T.; Rieger, R.; Mullen, K.; Rabe, J. P.; Zojer, E.; Koch, N. Gold Work Function Reduction by 2.2 EV with an Air-Stable Molecular Donor Layer. *Appl. Phys. Lett.* **2008**, *93*, 243303.
14. Love, J. C.; Estroff, L. A.; Kriebel, J. K.; Nuzzo, R. G.; Whitesides, G. M. Self-Assembled Monolayers of Thiolates on Metals as a Form of Nanotechnology. *Chem. Rev.* **2005**, *105*, 1103–1169.
15. Campbell, I. H.; Rubin, S.; Zawodzinski, T. A.; Kress, J. D.; Martin, R. L.; Smith, D. L.; Barashkov, N. N.; Ferraris, J. P. Controlling Schottky Energy Barriers in Organic Electronic Devices Using Self-Assembled Monolayers. *Phys. Rev. B* **1996**, *54*, 14321–14324.
16. Cahen, D.; Kahn, A. Electron Energetics at Surfaces and Interfaces: Concepts and Experiments. *Adv. Mater.* **2003**, *15*, 271–277.
17. Heimel, G.; Romaner, L.; Zojer, E.; Bredas, J.-L. The Interface Energetics of Self-Assembled Monolayers on Metals. *Acc. Chem. Res.* **2008**, *41*, 721–729.
18. Alloway, D. M.; Hofmann, M.; Smith, D. L.; Gruhn, N. E.; Graham, A. L.; Colorado, R.; Wysocki, V. H.; Lee, T. R.; Lee, P. A.; Armstrong, N. R. Interface Dipoles Arising from Self-Assembled Monolayers on Gold: UV-Photoemission Studies of Alkanethiols and Partially Fluorinated Alkanethiols. *J. Phys. Chem. B* **2003**, *107*, 11690–11699.
19. de Boer, B.; Hadipour, A.; Mandoc, M. M.; van Woudenbergh, T.; Blom, P. W. M. Tuning of Metal Work Functions with Self-Assembled Monolayers. *Adv. Mater.* **2005**, *17*, 621–625.
20. Heimel, G.; Romaner, L.; Zojer, E.; Bredas, J.-L. Toward Control of the Metal-Organic Interfacial Electronic Structure in Molecular Electronics: A First-Principles Study on Self-Assembled Monolayers of π-Conjugated Molecules on Noble Metals. *Nano Lett.* **2007**, *7*, 932–940.
21. Yip, H. L.; Hau, S. K.; Baek, N. S.; Ma, H.; Jen, A. K. Y. Polymer Solar Cells That Use Self-Assembled-Monolayer- Modified ZnO/Metals as Cathodes. *Adv. Mater.* **2008**, *20*, 2376–2382.
22. Mathijssen, S. G. J.; van Hal, P. A.; van den Biggelaar, T. J. M.; Smits, E. C. P.; de Boer, B.; Kemerink, M.; Janssen, R. A. J.; de Leeuw, D. M. Manipulating the Local Light Emission in Organic Light-Emitting Diodes by Using Patterned Self-Assembled Monolayers. *Adv. Mater.* **2008**, *20*, 2703–2706.
23. Halik, M.; Klauk, H.; Zschieschang, U.; Schmid, G.; Dehm, C.; Schuetz, M.; Effenberger, F.; Brunnbauer, M.; Stellacci, F. Low-Voltage Organic Transistors with an Amorphous Molecular Gate Dielectric. *Nature* **2004**, *431*, 963–966.
24. DiBenedetto, S. A.; Facchetti, A.; Ratner, M. A.; Marks, T. J. Molecular Self-Assembled Monolayers and Multilayers for Organic and Unconventional Inorganic Thin-Film Transistor Applications. *Adv. Mater.* **2009**, *21*, 1407–1433.
25. Zhou, Y.; Fuentes-Hernandez, C.; Shim, J.; Meyer, J.; Giordano, A. J.; Li, H.; Winget, P.; Papadopoulos, T.; Cheun, H.; Kim, J.; et al. Universal Method To Produce Low Work Function Electrodes for Organic Electronics. *Science* **2012**, *336*, 327–332.
26. Kumatani, A.; Li, Y.; Darmawan, P.; Minari, T.; Tsukagoshi, K. On Practical Charge Injection at the Metal/Organic Semiconductor Interface. *Sci. Rep.* **2013**, *3*, 1026.
27. Hofmann, S.; Thomschke, M.; Lussem, B.; Leo, K. Top-Emitting Organic Light-Emitting Diodes. *Opt. Express* **2011**, *19*, A1250–A1264.

28. Chen, L. M.; Xu, Z.; Hong, Z. R.; Yang, Y. Interface Investigation and Engineering—Achieving High Performance Polymer Photovoltaic Devices. *J. Mater. Chem.* **2010**, *20*, 2575–2598.
29. Ng, T. N.; Schwartz, D. E.; Lavery, L. L.; Whiting, G. L.; Russo, B.; Krusor, B.; Veres, J.; Bröms, P.; Herlogsson, L.; Alam, N., et al., Scalable Printed Electronics: An Organic Decoder Addressing Ferroelectric Non-volatile Memory. *Sci. Rep.* **2012**, *2*.
30. Ulman, A. *An Introducton to Ultrathin Organic Films*; Academic Press: 1991.
31. von Wrochem, F.; Gao, D.; Scholz, F.; Nothofer, H. G.; Nelles, G.; Wessels, J. M. Efficient Electronic Coupling and Improved Stability with Dithiocarbamate-Based Molecular Junctions. *Nat. Nanotechnol.* **2010**, *5*, 618–624.
32. Chidsey, C. E. D.; Liu, G. Y.; Rowntree, P.; Scoles, G. Molecular Order at the Surface of an Organic Monolayer Studied by Low-Energy Helium Diffraction. *J. Chem. Phys.* **1989**, *91*, 4421–4423.
33. Natan, A.; Zidon, Y.; Shapira, Y.; Kronik, L. Cooperative Effects and Dipole Formation at Semiconductor and Self-Assembled-Monolayer Interfaces. *Phys. Rev. B* **2006**, *73*, 193310.
34. A small fraction of physisorbed molecular rods oriented in the opposite direction towards the substrate might explain this effect as well, and this issue is currently under investigation.
35. Sirringhaus, H.; Brown, P. J.; Friend, R. H.; Nielsen, M. M.; Bechgaard, K.; Langeveld-Voss, B. M. W.; Spiering, A. J. H.; Janssen, R. A. J.; Meijer, E. W.; Herwig, P.; et al. Two-Dimensional Charge Transport in Self-Organized, High-Mobility Conjugated Polymers. *Nature* **1999**, *401*, 685–688.
36. Joseph Kline, R.; McGehee, M. D.; Toney, M. F. Highly Oriented Crystals at the Buried Interface in Polythiophene Thin-Film Transistors. *Nat. Mater.* **2006**, *5*, 222–228.
37. Fisher, J. C.; Giaever, I. Tunneling through Insulating Layers. *J. Appl. Phys.* **1961**, *32*, 172–177.
38. Lyon, J. E.; Cascio, A. J.; Beerbom, M. M.; Schlaf, R.; Zhu, Y.; Jenekhe, S. A. Photoemission Study of the Poly-(3-Hexylthiophene)/Au Interface. *Appl. Phys. Lett.* **2006**, *88*, 222109.
39. Wang, W. F.; Alsmeier, J. H.; Wolak, M.; Schlaf, R. Determination of the Charge Neutrality Level of Poly(3-hexylthiophene). *J. Chem. Phys.* **2013**, *138*, 054705.
40. Osikowicz, W.; de Jong, M. P.; Braun, S.; Tengstedt, C.; Fahlman, M.; Salaneck, W. R. Energetics at Au Top and Bottom Contacts on Conjugated Polymers. *Appl. Phys. Lett.* **2006**, *88*, 193504.
41. Kanai, K.; Miyazaki, T.; Suzuki, H.; Inaba, M.; Ouchi, Y.; Seki, K. Effect of Annealing on the Electronic Structure of Poly(3-Hexylthiophene) Thin Film. *Phys. Chem. Chem. Phys.* **2010**, *12*, 273–282.
42. Heeney, M.; Zhang, W.; Crouch, D. J.; Chabinyc, M. L.; Gordeyev, S.; Hamilton, R.; Higgins, S. J.; McCulloch, I.; Skabara, P. J.; Sparrowe, D.; *et al.* Regioregular Poly(3-hexyl)-selenophene: A Low Band Gap Organic Hole Transporting Polymer. *Chem.Commun.* **2007**, 5061–5063.
43. Scheinert, S.; Grobosch, M.; Paasch, G.; Horselmann, I.; Knupfer, M.; Bartsch, J. Contact Characterization by Photoemission and Device Performance in P3HT Based Organic Transistors. *J. Appl. Phys.* **2012**, *111*, 064502.
44. Lampert, M. A.; Mark, P. *Current Injection in Solids*; Academic: New York, 1970.
45. Tang, H.; Li, F.; Shinar, J. Bright High Efficiency Blue Organic Light-Emitting Diodes With Al_2O_3/Al Cathodes. *Appl. Phys. Lett.* **1997**, *71*, 2560–2562.
46. Iucci, G.; Xing, K.; Lögdlund, M.; Fahlman, M.; Salaneck, W. R. Polaron to Bipolaron Transition in a Conjugated Polymer. Rubidium-Doped Poly(*p*-phenylenevinylene). *Chem. Phys. Lett.* **1995**, *244*, 139–144.
47. Thankachan, C., Friedrich, K. J., Coker, D. E. Method of Making an Alkoxylated Polyethylenimine Product. U.S. Patent 7736525B2. 2010.
48. Chen, C. W.; Lin, C. L.; Wu, C. C. An Effective Cathode Structure for Inverted Top-Emitting Organic Light-Emitting Devices. *Appl. Phys. Lett.* **2004**, *85*, 2469–2471.
49. Burgi, L.; Richards, T. J.; Friend, R. H.; Sirringhaus, H. Close Look at Charge Carrier Injection in Polymer Field-Effect Transistors. *J. Appl. Phys.* **2003**, *94*, 6129–6137.
50. Wessels, J. M.; Nothofer, H. G.; Ford, W. E.; von Wrochem, F.; Scholz, F.; Vossmeyer, T.; Schroedter, A.; Weller, H.; Yasuda, A. Optical and Electrical Properties of Three-Dimensional Interlinked Gold Nanoparticle Assemblies. *J. Am. Chem. Soc.* **2004**, *126*, 3349–3356.
51. Zhao, Y.; Pérez-Segarra, W.; Shi, Q.; Wei, A. Dithiocarbamate Assembly on Gold. *J. Am. Chem. Soc.* **2005**, *127*, 7328–7329.
52. Gao, D.; Scholz, F.; Nothofer, H. G.; Ford, W. E.; Scherf, U.; Wessels, J.; Yasuda, A.; von Wrochem, F. Fabrication of Asymmetric Molecular Junctions by the Oriented Assembly of Dithiocarbamate Rectifiers. *J. Am. Chem. Soc.* **2011**, *133*, 5921–5930.